Research Square

Preprints are preliminary reports that have not undergone peer review.
They should not be considered conclusive, used to inform clinical practice,
or referenced by the media as validated information.

HSA-AIR: A Human-Centric Safety-Aware AI Framework for Reconfigurable Wearable Antennas toward 5G/6G Networks

PRABIR BANERJEE

prabir.banerjee@gmail.com

Heritage Institute of Technology https://orcid.org/0000-0001-8198-1397

Sabyasachi Chatterjee

Heritage Institute of Technology

Research Article

Keywords: wearable antenna, 6G, reconfigurable antenna, human safety, absorbed power density, SAR, bioheat, agentic AI, closed-loop optimization

Posted Date: November 10th, 2026

DOI: https://doi.org/10.21203/rs.3.rs-11663920/v1

License: This work is licensed under a Creative Commons Attribution 4.0 International License.
Read Full License

Additional Declarations: The authors declare no competing interests.

HSA-AIR: A Human-Centric Safety-Aware AI Framework for Reconfigurable Wearable Antennas toward 5G/6G Networks

Prabir Banerjee, Sabyasachi Chatterjee
Electronics and Communication Engineering Department
Heritage Institute of Technology, Kolkata

Abstract—Wearable antennas are expected to support increasingly dense sensing, communication, and human–machine interaction in beyond-5G and emerging 6G systems. Their proximity to the body, however, makes electromagnetic exposure, tissue heating, body-induced detuning, motion, and energy consumption inseparable from conventional RF objectives. This paper proposes HSA-AIR, a human-centric safety-aware AI-controlled reconfiguration framework in which human exposure is treated as a hard admissibility condition rather than only a post-design verification metric. The controller senses human and channel states, predicts electromagnetic and thermal consequences, rejects unsafe candidate actions, and then optimizes RF utility over the remaining safe action set. Reconfiguration variables include varactor bias, radiation-pattern state, transmit power, and frequency mode. A physics-informed simulation and validation suite is used to compare HSA-AIR with fixed, RF-only, and safety-power controllers. In a 50-step dynamic scenario, HSA-AIR reduced mean absorbed-power-density (APD) proxy by 46.8% relative to fixed operation with only about 2.0% reduction in mean throughput proxy. A 1000-trial Monte-Carlo study yielded a 98.4% joint safety-and-RF pass probability, mean APD proxy of 1.049 W/m², mean effective SNR of 13.79 dB, and mean transmit power of 34.4 mW. Physics-consistency tests achieved 100% pass rate, while an independent one-dimensional Pennes bioheat model confirmed the monotonic thermal behavior of the surrogate. The results support the feasibility of safety-first closed-loop wearable-antenna control, while full-wave electromagnetic and experimental validation remain necessary before regulatory safety claims.

Keywords—wearable antenna, 6G, reconfigurable antenna, human safety, absorbed power density, SAR, bioheat, agentic AI, closed-loop optimization.

I. INTRODUCTION

Wearable radios are moving from relatively low-rate body-area links toward high-capacity sensing, extended-reality, medical telemetry, industrial assistance, localization, and human–machine interfaces. This evolution makes antenna design increasingly difficult because the radiator is not operating in free space: it is electromagnetically coupled to a lossy, dispersive, moving, and thermally active human body. The same antenna may therefore exhibit different resonance, efficiency, pattern, and exposure characteristics when placed on the wrist, arm, chest, shoulder, or back, or when the body bends and the antenna-to-skin separation changes. [11], [12], [14], [16]

Recent wearable-antenna research has demonstrated low-SAR structures, metasurface and AMC isolation, flexible substrates, frequency/polarization reconfiguration, and machine-learning-assisted design. A recent 3.5/28-GHz wearable antenna, for example, combines PIN-diode reconfiguration, measured RF performance, on-body/bending evaluation, SAR assessment, and supervised ML prediction [4]. These developments are important, but the safety calculation is still typically performed after a geometry or operating state has been selected. HSA-AIR changes the control hierarchy: exposure and thermal constraints are evaluated before an RF-optimal action is allowed. [11]–[14], [19]

The contribution of this conference paper is intentionally focused. It presents the safety-first HSA-AIR architecture, its physics-informed control model, a compact quantitative comparison against three controller baselines, and a validation suite comprising physical monotonicity checks, Monte-Carlo robustness,

independent bioheat cross-validation, and disturbance–recovery testing. The article does not claim regulatory compliance; instead, it establishes a reproducible control-level foundation suitable for subsequent full-wave and experimental validation.

II. PHYSICAL BASIS AND RESEARCH GAP

A. Body Coupling and Exposure

For a wearable source, body proximity modifies both the antenna impedance and the distribution of electromagnetic energy. At frequencies above 6 GHz, energy deposition becomes increasingly superficial and absorbed power density is an important dosimetric quantity under the applicable averaging definitions [1]. Near-field wearable exposure cannot be inferred reliably from a simple far-field power-density expression alone; consequently, the present model uses an APD proxy for controller development and explicitly reserves standards-compliant assessment for full-wave validation. [1], [18]

$$S_inc \approx P_t\eta_b/(4\pi d_eff^2) \qquad (1)$$

Here P_t is transmit power, η_b is an effective body-directed coupling factor, and d_eff is an effective antenna-body separation. Although (1) is a reduced-order relationship, it preserves the expected monotonic dependence of exposure on transmit power, pattern orientation, placement, and separation. At millimetre-wave frequencies, anatomical detail becomes important: recent 28-GHz FDTD analysis reported that homogeneous-skin models produced wearable-source APD values 16–30% lower than stratified-skin models [3]. This motivates the multilayer validation pathway in HSA-AIR.

B. Thermal Coupling

Electromagnetic absorption is relevant because deposited RF energy acts as a heat source. A higher-fidelity thermal model can be expressed using the Pennes bioheat equation: [10], [15], [20]

$$\rho c\partial T/\partial t = \nabla \cdot (k\nabla T) + \rho_b c_b \omega_b (T_b - T) + Q_met + Q_E M \qquad (2)$$

$$Q_E M = \rho \cdot SAR \qquad (3)$$

The control simulator uses a fast temperature-rise surrogate, while the validation suite independently solves a one-dimensional skin–fat–muscle Pennes model. This separation is useful because the controller can remain computationally lightweight while a more physical model checks whether its thermal trend is credible.

C. Gap in Recent AI-Assisted Wearable Antennas

AI is increasingly used for antenna topology generation, surrogate prediction, parameter optimization, adaptive beamforming, and reconfigurable control [7]. However, combining human-state sensing, exposure prediction, thermal screening, hard safety constraints, RF optimization, multi-actuator reconfiguration, verification, and fail-safe operation in one wearable-antenna loop remains insufficiently explored. HSA-AIR is positioned at this integration gap rather than claiming novelty for any single component. [7], [12]

III. HSA-AIR SAFETY-FIRST ARCHITECTURE

The controller operates as a repeated sense–predict–gate–optimize–act–verify loop. At control instant k, the state vector includes posture, placement, body gap, moisture, motion, skin/ambient temperature, target frequency, channel SNR, and traffic priority. Candidate actions combine varactor bias, pattern state, transmit power, and frequency mode:

$$A = V \times P \times S_p \times F \qquad (4)$$

The present pattern states are OUTWARD, BALANCED, and OMNI. OUTWARD is assigned the lowest body-coupling factor and a positive outward-link gain contribution. Varactor tuning provides fine resonance correction, with capacitance represented by the usual junction relation [11], [13]

$$C_V(V_B) = C_0/\left(1 + V_B/V_J\right)^m \qquad (5)$$

and the resonance shift approximated through the effective LC dependence. Candidate actions are evaluated first for exposure and temperature. A hard safety gate removes inadmissible states:

$$G_safe(a,k) = 1 if APD \le APD_max, \Delta T \le \Delta T_max, T_skin \le T_max; else 0 \qquad (6)$$

Only candidates that survive (6) are evaluated by the RF gate:

$$G_RF(a,k) = 1ifS11 \leq -10dBandSNR_eff \geq 10dB; else0 \qquad (7)$$

The remaining candidates are ranked by a human-centric utility containing safety, thermal, power, pattern, matching, SNR, throughput, and switching-cost terms. The baseline weighting is

$$J* = max_a\left[0.55J_H + 0.40J_RF + 0.05J_QoS - J_sw\right] \qquad (8)$$

This lexicographic structure is central to the proposal. An unsafe state cannot become acceptable merely because it offers high gain or throughput. If no state passes both gates, the controller enters FAIL_SAFE mode, selects outward radiation, and reduces transmit power.

Human + Channel State → Exposure/Thermal Predictor → HARD SAFETY GATE → RF Gate & Utility → Reconfiguration → Verification / Feedback

Fig. 1. Functional sequence of the HSA-AIR closed-loop controller.

IV. SIMULATION AND VALIDATION METHODOLOGY

The baseline experiment uses research study points at 7.5, 15, and 28 GHz; these are not asserted as final 6G allocations. The principal dynamic experiment uses a 50-step sequence containing standing, walking, bending, running, and sitting intervals. The baseline placement is the back with a 10.5-mm antenna-body gap. Candidate varactor bias spans 0–12 V; transmit powers are 10, 20, 35, 50, 70, and 100 mW; and the three pattern states are searched exhaustively. [12], [16]

Four controller cases are evaluated under common conditions: a fixed 50-mW BALANCED antenna; an RF-only controller that maximizes matching/SNR/throughput without an exposure penalty; a safety-power controller using OUTWARD radiation and the minimum usable power; and the complete HSA-AIR controller. This ablation separates the contribution of safety screening from simple power reduction.

The Validation Suite V1.0 adds four independent checks. First, physics-consistency tests verify monotonic relationships involving transmit power, body gap, varactor capacitance, resonance, thermal response, and pattern direction. Second, 1000 randomized trials per controller vary posture, placement, gap, moisture, temperature, motion, and channel SNR. Third, a one-dimensional multilayer Pennes solver independently evaluates RF-induced temperature rise relative to a zero-RF thermal baseline. Fourth, a disturbance experiment abruptly changes posture, gap, moisture, and SNR to test recovery. Table I represents the principal simulation parameters that have been analysed in this paper.

Table I. Principal simulation parameters

Parameter	Baseline	Role
Body gap	10.5 mm	Coupling/exposure
Bias	0–12 V	Resonance tuning
Power	10–100 mW	RF/safety control
Patterns	Outward/Balanced/Omni	Body isolation
S11 gate	≤ −10 dB	Matching
SNR gate	≥ 10 dB	Link usability
MC trials	1000/controller	Robustness

.

V. RESULTS AND HUMAN-SAFETY ANALYSIS

A. Dynamic Ablation Results

In the common 50-step scenario, HSA-AIR achieved a mean APD proxy of 0.477 W/m² and a peak value of 0.708 W/m². Fixed operation produced 0.897 and 1.044 W/m², respectively. Thus HSA-AIR reduced mean APD by approximately 46.8% and peak APD by approximately 32.2% relative to fixed operation. The RF-only controller produced still higher exposure because its optimization naturally favored high transmit power.

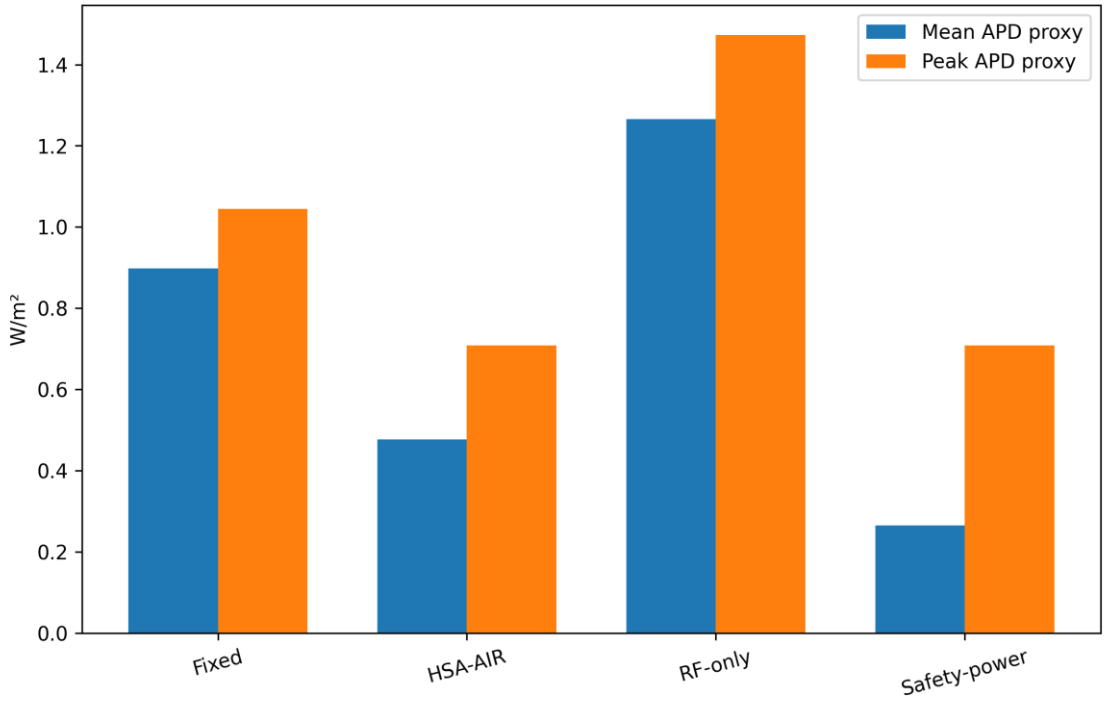


Fig. 2. Mean and peak APD proxies in the deterministic ablation experiment.

The exposure reduction was not obtained by simply collapsing link performance. HSA-AIR maintained a minimum effective SNR of 10.08 dB with no RF outage in the 50 evaluated states. Its mean effective SNR was 15.39 dB and mean throughput proxy was 5.17. The fixed controller achieved a mean throughput proxy of 5.28; therefore the approximately 46.8% reduction in mean APD was accompanied by only about a 2.0% reduction in mean throughput proxy.

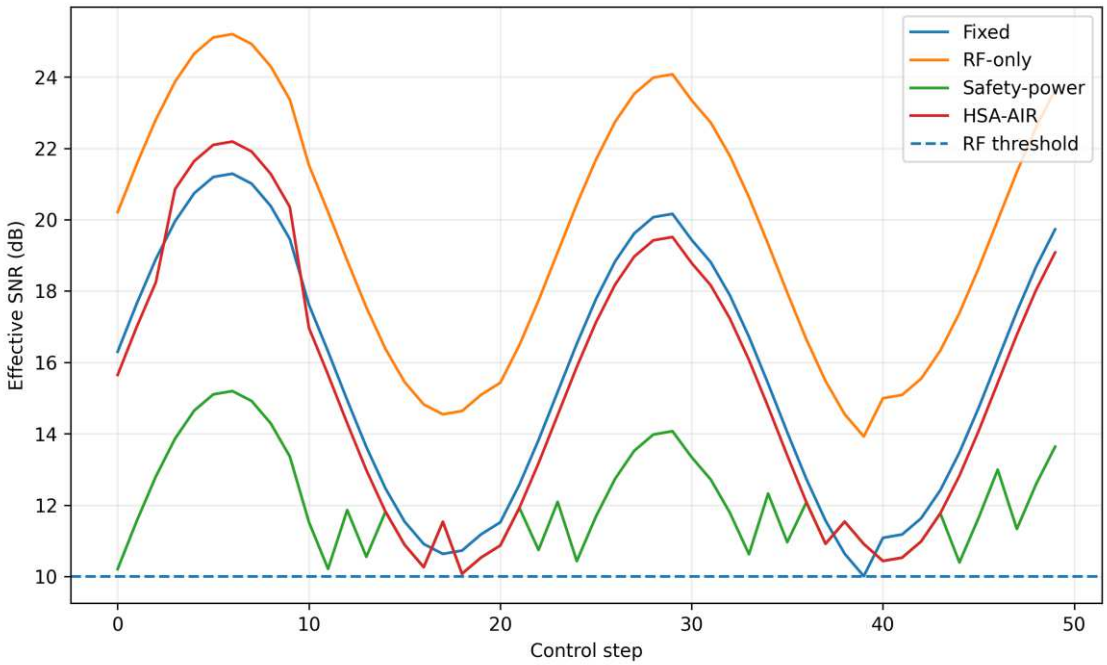


Fig. 3. Effective SNR under the four controller strategies.

Mean transmit power provides another important interpretation. HSA-AIR used 38 mW on average, compared with 50 mW for fixed operation and 100 mW for RF-only adaptation. The safety-power controller used only 20.7 mW and achieved the lowest APD, but its mean effective SNR fell to 12.02 dB. HSA-AIR should therefore be viewed as a safety-conscious high-utility controller, not as an absolute exposure minimizer.

B. Monte-Carlo Robustness

The randomized validation is more demanding because the controller must handle a distribution of human and channel states rather than one predetermined trajectory. Across 1000 trials per controller, HSA-AIR achieved a 98.4% joint safety-and-RF pass probability. Its mean APD proxy was 1.049 W/m², 95th-percentile APD was 2.227 W/m², mean effective SNR was 13.79 dB, and mean transmit power was 34.4 mW.

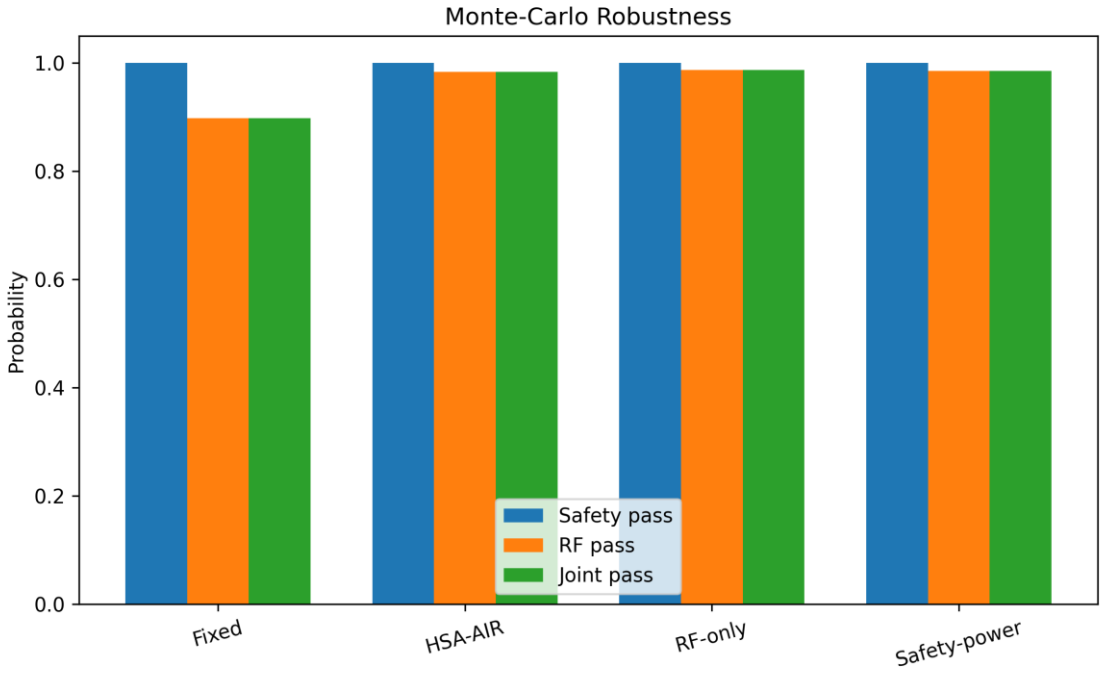


Fig. 4. Monte-Carlo safety, RF-usability, and joint-pass probabilities.

The fixed controller achieved only 89.8% RF usability under the randomized states. RF-only control achieved 98.7% RF usability but at approximately 98.0 mW mean transmit power and 3.134 W/m² mean APD proxy. Safety-power control achieved 98.5% joint pass and the lowest mean APD, but its mean SNR was only 11.64 dB. These results reinforce the same trade-space observed in the deterministic study.

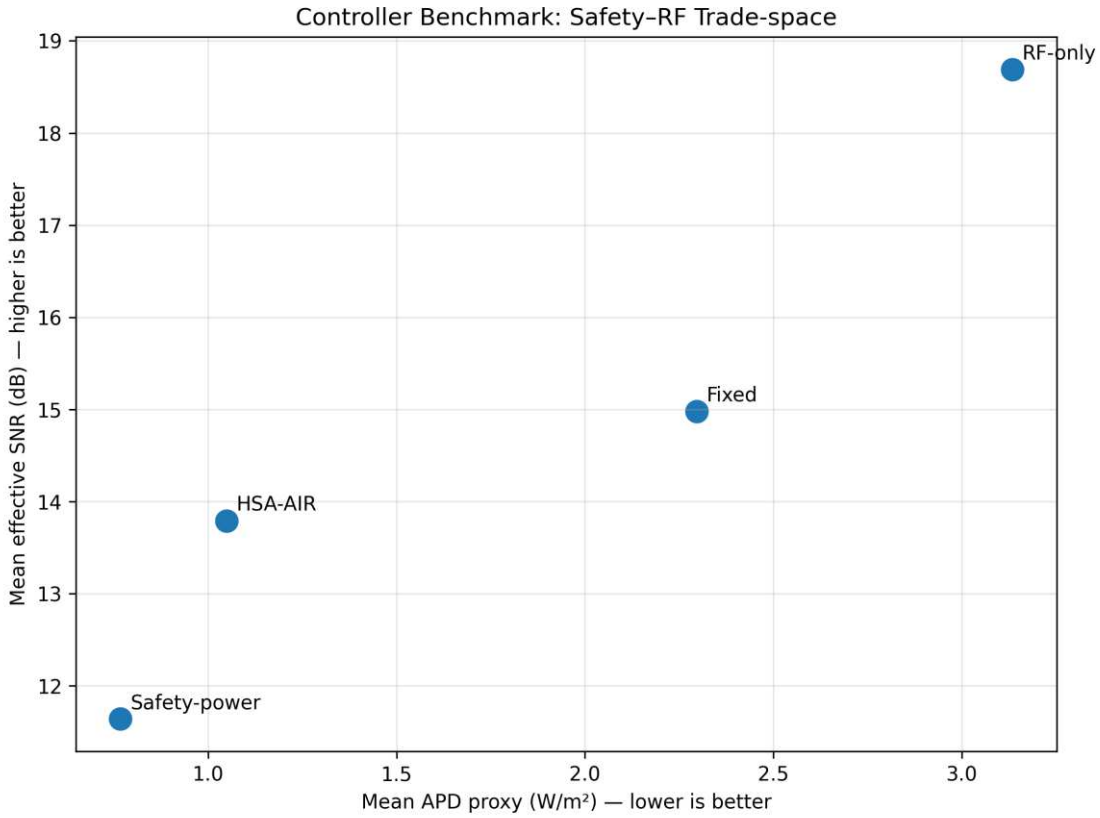


Fig. 5. Safety–RF trade-space from the randomized controller benchmark.

C. Physics and Thermal Cross-Validation

All seven physics-consistency tests passed, giving a 100% Physics Consistency Score. Specifically, the model preserved increasing APD with transmit power, decreasing APD with body gap, decreasing varactor capacitance with reverse bias, increasing resonance with bias for the selected tuning model, increasing temperature-rise proxy with APD, and the expected OUTWARD < BALANCED < OMNI body-exposure ordering. A 500-case randomized APD–power monotonicity test also passed.

The independent Pennes model provides a second type of evidence. Over an APD sweep of 0.1–5 W/m², the HSA-AIR temperature surrogate and the Pennes RF-induced temperature rise were perfectly monotonic with Pearson r=1.0. Their raw RMSE was 0.0163 °C; a linear calibration slope of 0.695 aligned the surrogate with the independent model. This should not be interpreted as full thermal validation because both models still depend on assumed tissue properties and reduced-order EM deposition. It does show that the fast controller surrogate preserves the correct thermal ordering and can be calibrated to a higher-fidelity solver.

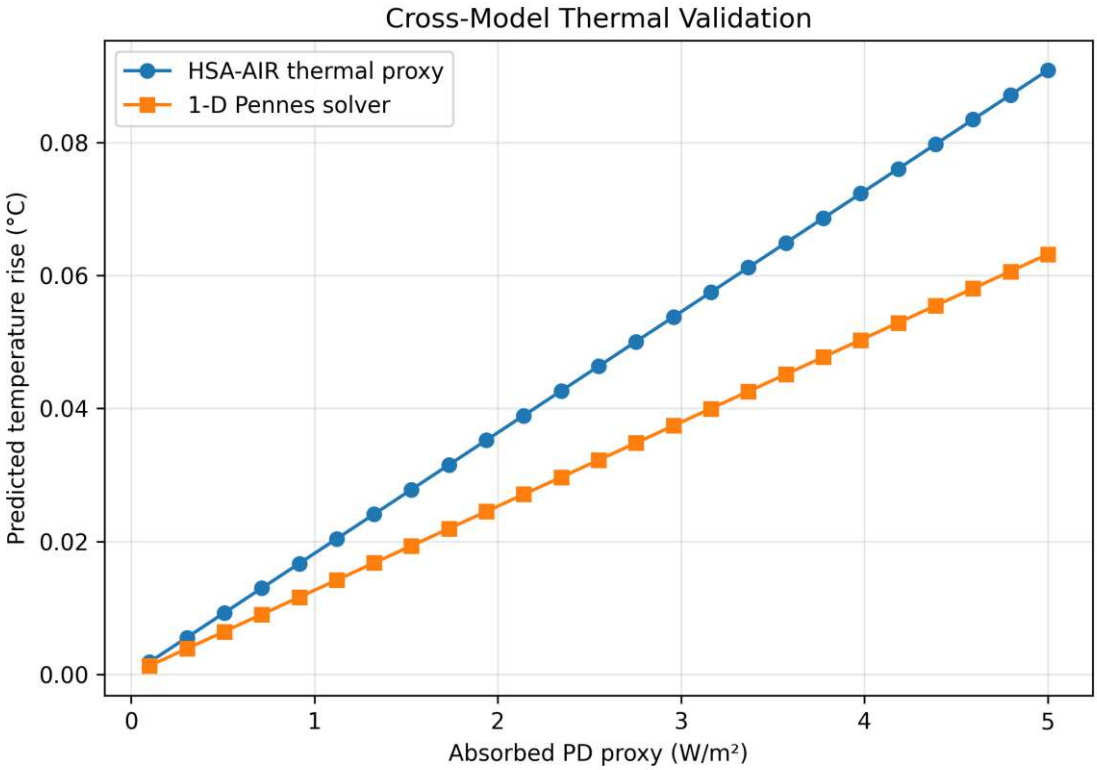


Fig. 6. Cross-model thermal validation: controller surrogate versus 1-D Pennes model.

VI. NOVELTY AND COMPARISON WITH RECENT WORK

The novelty claim must be framed carefully because recent literature already contains AI-optimized wearable antennas, reconfigurable wearable antennas, low-SAR structures, realistic APD studies, and electromagnetic–thermal analyses. Salisu et al. combined 3.5/28-GHz frequency reconfiguration with supervised ML, bending/on-body tests, and SAR evaluation [4]. Gallucci et al. demonstrated the sensitivity of 28-GHz APD to anthropomorphic shape and skin stratification [3]. Broader AI-antenna literature now includes surrogate optimization and reinforcement-learning control [7]. HSA-AIR therefore does not claim priority for these individual ingredients. [4], [11]–[14], [17], [19]. Table II compares HSA-AIR results with respect to some important parameters.

Its contribution is the control hierarchy: human state and channel state enter the same decision process; exposure and thermal quantities define a hard admissible set; RF utility is optimized only within that set; several antenna actuators are coordinated; the chosen action is verified; and a fail-safe state is defined. In representative recent wearable studies, safety is generally evaluated as a design or validation output rather than as a pre-action runtime gate.

Table II. Compact feature-level positioning of HSA-AIR.

Approach	Reconfig.	AI	Body safety	Safety gate	Closed loop
ML wearable [4]	Freq.	Yes	SAR	No	No
28-GHz dosimetry [3]	No	No	APD	No	No
Low-SAR wearable class	Passive	Optional	SAR	No	No
HSA-AIR	Bias/pattern/power/band	Agentic	APD+thermal pathway	YES	YES

VII. DISCUSSION, LIMITATIONS, AND VALIDATION ROADMAP

The results expose a three-way Safety–RF–Energy trade-space. RF-only optimization moves toward high power and high SNR; safety-power control moves toward minimum exposure but operates closer to the RF boundary; HSA-AIR selects an intermediate state with additional RF margin while retaining substantially lower exposure than fixed or RF-only operation. This is a useful operating philosophy for wearable radios because channel conditions and body coupling are time varying.

The present work nevertheless remains a simulation-level demonstration. APD and S11 are physics-informed surrogates rather than outputs from a full-wave human-body model. The thermal cross-validation uses a one-dimensional Pennes solver and simplified RF deposition. The 7.5, 15, and 28-GHz points are research frequencies, not claims about finalized 6G spectrum. Consequently, the numerical APD values should not be presented as evidence of regulatory compliance.

The next validation stage is explicit. First, the optimized antenna states should be solved in HFSS, CST, FEKO, openEMS, or another validated full-wave environment using multilayer and anatomically realistic phantoms. The comparison should include resonance frequency, S11, gain, efficiency, pattern, APD/SAR, and body detuning. Second, the full-wave heat source should drive a three-dimensional bioheat model. Third, a subset of states should be fabricated and tested in free space and with suitable phantoms. These data can then recalibrate the fast surrogate and quantify simulation-to-reality uncertainty. [3], [10], [13], [20]

A further research direction is safe reinforcement learning. The current exhaustive search is transparent and useful for validation, but the action space will grow rapidly if beam states, tunable metasurfaces, multiple frequency channels, and user-specific body models are introduced. A constrained RL or model-predictive controller could learn efficient policies while retaining an independent safety shield. Explainability is also important: a wearable safety controller should report why a candidate was rejected and which variable triggered a fail-safe transition.

VIII. CONCLUSION

This paper introduced HSA-AIR, a human-centric safety-aware AI framework for reconfigurable wearable antennas intended for beyond-5G/6G research. The key idea is to move human safety from post-design verification into the antenna decision loop. Candidate configurations are screened by electromagnetic and thermal constraints before RF utility is optimized. In deterministic ablation, HSA-AIR reduced mean APD proxy by 46.8% relative to fixed operation with only about 2.0% reduction in mean throughput proxy. In 1000 randomized trials, it achieved 98.4% joint safety-and-RF pass probability with 34.4 mW mean transmit power. Physics-consistency and independent bioheat checks further support the internal credibility of the framework. The results justify continued development, but full-wave and experimental validation are required before quantitative human-safety or compliance claims. The principal contribution is therefore a validated control architecture for safety-first adaptive wearable antennas rather than a claim of final regulatory performance.

REFERENCES

[1] ICNIRP, "Guidelines for limiting exposure to electromagnetic fields (100 kHz to 300 GHz)," Health Physics, vol. 118, no. 5, pp. 483–524, 2020.

[2] "A comprehensive review of recent methods for compactness and performance enhancement in 5G and 6G wearable antennas," Alexandria Engineering Journal, vol. 95, pp. 132–163, 2024, doi: 10.1016/j.aej.2024.03.097.

[3] S. Gallucci et al., "Impact of Anthropomorphic Shape and Skin Stratification on Absorbed Power Density in mmWaves Exposure Scenarios," Sensors, vol. 25, no. 14, Art. 4461, 2025, doi: 10.3390/s25144461.

[4] A. Salisu et al., "Machine learning-optimized compact wearable frequency reconfigurable antenna for sub-6 GHz/mm-wave 5G integration," Scientific Reports, vol. 15, Art. 44912, 2025, doi: 10.1038/s41598-025-28971-x.

[5] U. Musa et al., "Machine learning-optimized dual-band wearable antenna for real-time remote patient monitoring in biomedical IoT systems," Scientific Reports, vol. 15, 2025.

[6] "Broadband Dual-Sense Circular-Polarization Reconfigurable Metasurface Antenna for Wearable Applications," IEEE Access, vol. 13, pp. 130138–130146, 2025, doi: 10.1109/ACCESS.2025.3590767.

[7] W. Xu et al., "The evolving landscape of AI-powered antenna design, optimization, and control: A comprehensive review," Ain Shams Engineering Journal, vol. 17, no. 3, Art. 104052, 2026, doi: 10.1016/j.asej.2026.104052.

[8] "Assessment of EMF Human Exposure Levels Due to Wearable Antennas at 5G Frequency Band," Sensors, 2023.

[9] "Implantable antenna for biomedical applications: electromagnetic, SAR, and thermal performance evaluation," Scientific Reports, 2025, doi: 10.1038/s41598-025-21600-7.

[10] H. H. Pennes, “Analysis of tissue and arterial blood temperatures in the resting human forearm,” Journal of Applied Physiology, vol. 1, no. 2, pp. 93–122, 1948. doi: 10.1152/jappl.1948.1.2.93.

[11] K. N. Paracha, S. K. A. Rahim, P. J. Soh, and M. Khalily, “Wearable antennas: A review of materials, structures, and innovative features for autonomous communication and sensing,” IEEE Access, vol. 7, pp. 56694–56712, 2019. doi: 10.1109/ACCESS.2019.2909146.

[12] S. Saleh, T. Saeidi, N. Timmons, and F. Razzaz, “A comprehensive review of recent methods for compactness and performance enhancement in 5G and 6G wearable antennas,” Alexandria Engineering Journal, vol. 95, pp. 132–163, 2024. doi: 10.1016/j.aej.2024.03.097.

[13] G. K. Soni, D. Yadav, A. Kumar, A. Rathi, and S. V. Yadav, “Design of a compact multistubs resonator based dual-band flexible wearable antenna with low SAR for sub-6 GHz ISM applications,” Scientific Reports, vol. 15, art. 24013, 2025. doi: 10.1038/s41598-025-07724-w.

[14] S. R. Kale and D. P. Patil, “A Review of Wearable Antennas for 5G and Body-Centric Wireless Communication,” Devices and Methods of Measurements, vol. 15, no. 4, pp. 269–286, 2024. doi: 10.21122/2220-9506-2024-15-4-269-286.

[15] H. H. Pennes, “Analysis of tissue and arterial blood temperatures in the resting human forearm,” Journal of Applied Physiology, vol. 85, no. 1, pp. 5–34, 1998 (historical reprint). doi: 10.1152/jappl.1998.85.1.5.

[16] “A road towards 6G communication—a review of 5G antennas, arrays, and wearable devices,” Electronics, vol. 11, art. 169, 2022. doi: 10.3390/electronics11010169.

[17] “A circularly polarized sub-terahertz antenna with low-profile and high-gain for 6G wireless communication systems,” IEEE Access, vol. 9, p. 122607 et seq., 2021. doi: 10.1109/ACCESS.2021.3109161.

[18] “An overview of terahertz antennas,” China Communications, vol. 17, 2020. doi: 10.23919/J.CC.2020.07.011.

[19] “Flexible MIMO Antennas for 5G Applications,” in Proc. ICETET-SIP, IEEE, 2022. doi: 10.1109/ICETET-SIP-2254415.2022.9791704.
[20] “Pennes’ 1948 paper revisited,” Journal of Applied Physiology, vol. 85, no. 1, pp. 35 onward, 1998. doi: 10.1152/jappl.1998.85.1.35.